

# Van-Hove tuning of Fermi surface instabilities through compensated metallicity

Hendrik Hohmann,<sup>1,2</sup> Matteo Dürrnagel,<sup>1,2,3</sup> Matthew Bunney,<sup>4,5</sup> Stefan Enzner,<sup>1,2</sup> Tilman Schwemmer,<sup>1</sup> Titus Neupert,<sup>6</sup> Giorgio Sangiovanni,<sup>1,2</sup> Stephan Rachel,<sup>2,4</sup> and Ronny Thomale<sup>1,2,\*</sup>

<sup>1</sup>*Institute for Theoretical Physics and Astrophysics,  
University of Würzburg, D-97074 Würzburg, Germany*

<sup>2</sup>*Würzburg-Dresden Cluster of Excellence ct.qmat, Germany*

<sup>3</sup>*Institute for Theoretical Physics, ETH Zürich, 8093 Zürich, Switzerland*

<sup>4</sup>*School of Physics, University of Melbourne, Parkville, VIC 3010, Australia*

<sup>5</sup>*Institute for Theoretical Solid State Physics, RWTH Aachen University, 52062 Aachen, Germany*

<sup>6</sup>*Department of Physics, University of Zürich, Winterthurerstrasse 190, Zurich, Switzerland*

(Dated: December 23, 2024)

Van-Hove (vH) singularities in the vicinity of the Fermi level facilitate the emergence of electronically mediated Fermi surface instabilities. This is because they provide a momentum-localized enhancement of density of states promoting selective electronic scattering channels. High-temperature topological superconductivity has been argued for in graphene at vH filling which, however, has so far proven inaccessible due to the demanded large doping from pristine half filling. We propose compensated metallicity as a path to unlock vH-driven pairing close to half filling in an electronic honeycomb lattice model. Enabled by an emergent multi-pocket fermiology, charge compensation is realized by strong breaking of chiral symmetry from intra-sublattice hybridization, while retaining vH dominated physics at the Fermi level. We conclude by proposing tangible realizations through quantum material design.

*Introduction* At sufficiently low temperature, metals as interacting many-body electron systems tend to seek a minimization of ground state energy through spontaneous symmetry breaking. Starting from a Fermi surface (FS) configuration, the metal can become unstable upon the formation of electronic order related to magnetism, charge order, superconductivity, nematicity, and more. Already from earliest descriptions of electronic collective phenomena such as the Stoner criterion for itinerant ferromagnetism or BCS superconductivity, the propensity for FS instabilities generically depends on the ordering's channel-specific coupling strength and the density of states (DoS) at the Fermi level [1, 2]. The latter is intuitive from a Hamiltonian spectral flow perspective: The more spectral weight is pushed away from the Fermi level the more the ground state can be pushed down in energy. Van-Hove singularities (vHs) at or close to the Fermi level are particularly useful to elevate instability scales of electronic order, and are a crucial ingredient to theories of electronic materials. While the clean limit of vHs in two spatial dimensions features a logarithmically diverging DoS at specific points in momentum space, their realization in an imperfect quantum electronic material still ensures a peak in DoS at the vH points.

As many electronic kinetic models naturally feature vH points, it is particularly desirable to devise ways to tune the vH points of a given band structure to the Fermi level in order to facilitate the emergence of vH-driven FS instabilities. Pressure has some tuning impact on vH points, but also implies side-effects to electronic bands some of which would reduce the FS instability scales by reducing the interaction vs. bandwidth ratio [3]. Doping is another established way of tuning the vH profile. Unless

it is constrained to a few percent of doping that could be accomplished via electrolytic gating, however, chemical doping likewise has negative side-effects on FS instability scales such as the enhancement of disorder [4–6].

In this Letter, we propose an alternative principle to perform vH engineering in a model of interacting electrons on lattices with honeycomb structure. Rather than external pressure or doping, we propose *compensated metallicity* to deform a Fermi pocket towards the vH points around pristine half filling. We show how the absence of chiral symmetry due to intra-sublattice hybridization facilitates the emergence of a circular electron pocket (ep) at the Brillouin zone (BZ) center and an enlarged hole pocket (hp) tuned into proximity to the vH points at  $M$ . While the scattering vertex contributions of the ep turn out to be of marginal significance due to its isotropic character, the vH-proximitized hp triggers ideal conditions for the unfolding of unconventional FS instabilities. Deriving from ab-initio simulations we substantiate our proposed charge compensation principle by suggesting strained Xene structures [7, 8] (*i.e.* silicene, germanene, stanene) as possible material realizations.

*Honeycomb Hubbard model* To illustrate vH-tuning assisted by compensated metallicity, we study the  $t_1$ - $t_2$ - $U$  tight-binding Hubbard model on the honeycomb lattice

$$\hat{H} = \left( -t_1 \sum_{\langle i,j \rangle \sigma} \hat{c}_{i\sigma}^\dagger \hat{c}_{j\sigma} - t_2 \sum_{\langle\langle i,j \rangle\rangle \sigma} \hat{c}_{i\sigma}^\dagger \hat{c}_{j\sigma} \right) + \text{h.c.} - \mu \sum_{i\sigma} \hat{n}_{i\sigma} + U \sum_i \hat{n}_{i\uparrow} \hat{n}_{i\downarrow}, \quad (1)$$

where  $\hat{c}_{i\sigma}^{(\dagger)}$  denotes electron annihilation (creation) operators at site  $i$  with spin  $\sigma$  and  $\hat{n}_{i\sigma} = \hat{c}_{i\sigma}^\dagger \hat{c}_{i\sigma}$ ,  $U > 0$  is the onsite Coulomb repulsion, and  $\mu$  denotes the chemical

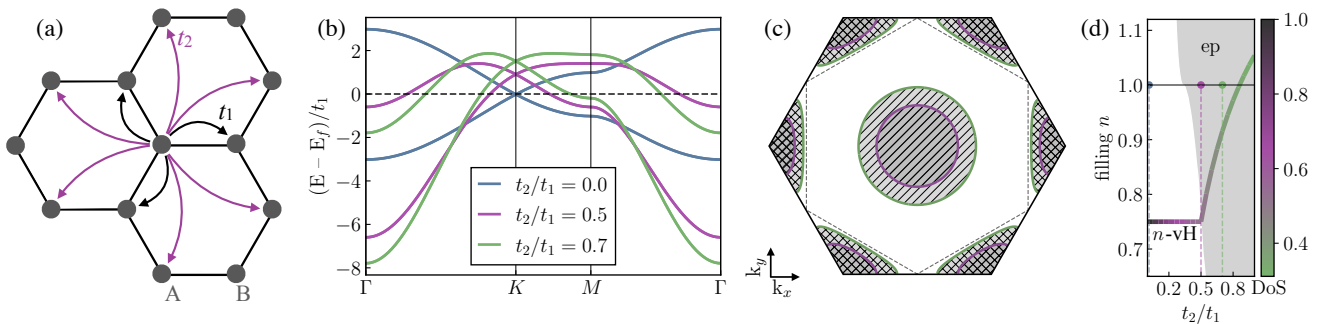


**Figure 1.** *Absence of chiral symmetry and compensated metallicity* (a) Real space lattice structure and hybridization elements of the honeycomb Hubbard model, as given in Eq. 1. (b) Single particle dispersion of the kinetic terms of Eq. 1. Finite next-nearest neighbor hybridization breaks particle-hole symmetry and shifts the lower van-Hove singularity towards the Fermi level at half filling (dashed line). (c) Fermi surfaces at half filling within the hexagonal BZ, corresponding to the  $t_2/t_1$  hopping values shown in (b). Electron (hole) pockets are indicated by crossed (diagonal) hatching. The perfectly nested outer FS is indicated by dashed line. (d) Lower vH filling and associated DoS at the Fermi level as a function of  $t_2/t_1$ . The dashed lines indicate  $t_2/t_1$  values of (b) and (c). The opening of the electron pocket (ep) around  $\Gamma$  (gray) shifts the vH towards pristine half filling ( $n = 1$ ). The numeric density of states (DOS) at an interval around vH is indicated along the vH line.

potential. The (next) nearest neighbor hopping elements  $t_1$  ( $t_2$ )  $> 0$  are visualized in Figure 1(a) as to how they realize (intra-) inter-sublattice hybridization.

Eq. 1 provides an effective model for graphene monolayers [9, 10]. Diagonalizing the kinetic part of Eq. 1 in the limit  $t_2 \ll t_1$ , where there is only orbital hybridization between the  $p_z$  orbitals of neighboring carbon atoms, a large nested Fermi pocket is realized at van-Hove fillings  $n = 3/4, 5/4$ , with a point-like FS hosting Dirac points at half filling  $n = 1$ . These values are pinned by the chiral symmetry of the bipartite honeycomb lattice,  $\{\hat{H}, \hat{C}\} = 0$ , where  $\hat{C} = \hat{P} \cdot \hat{T}$  is defined as the combination of particle-hole ( $\hat{P}$ ) and time-reversal ( $\hat{T}$ ) symmetry and can be represented as the third Pauli matrix acting on the sublattice degree of freedom in Eq. (1) [11]. The chiral symmetry of the energy spectrum is broken by imposing finite intra-sublattice hybridization  $t_2$  in Figure 1(b).

Due to the high quality of graphene samples, where lattice distortions or vacancies are rare, the clean limit given in Eq. (1) bears significant resemblance to the experimental setting. A major factor inhibiting the observation of a FS instability in graphene is the small DoS around pristine filling. Tuning graphene to a vH level is therefore an alluring path towards enhancing electronic order, and has been extensively discussed in the literature as a route to promote electronically mediated pairing [12–17]. It is expected to yield a chiral  $d$ -wave gapped superconductor, which is a topologically ordered quantum many-body state, *i.e.*, a Chern-Bogoliubov band insulator with Majorana edge modes [18–22]. The realization of such a state has, however, thus far been elusive, since homogeneously doping graphene to such high fillings unavoidably induces a critical amount of disorder to suppress such desired electronic instabilities [4, 5].

*Van-Hove tuning from compensated metallicity* As opposed to the single pocket case, a multi-pocket fermiology

can enable the transfer of charges between Fermi sheets with electron and hole character, in compliance with the Luttinger theorem [23, 24]. In the last decade, this has been extensively discussed in the case of the iron pnictides [25–27]. In such compounds, an increase of the number of conduction band electrons is compensated for by increasing the occupation of hole states in the valence band. This creates a compensated metal – an overall charge neutral compound with a large ensemble of low-energy hole-type and electron-type excitations at pristine filling, and possibly enhanced nesting effects between eps and hps at and off the Fermi level [28–30].

We find that a key step along the path towards compensated metal phases in a honeycomb lattice model described by Eq. 1 is the assumption of sizable  $t_2$ , which creates an asymmetry between the two vHs (Figure 1(b)). The energy bands are flattened and pushed up in energy at the BZ boundary, while significant  $t_2$  exhibits the opposite effect around the BZ center  $\Gamma$ , introducing an electron pocket at half-filling for  $t_2 > t_1/3$ . By inducing this Lifshitz transition, we allow the point-like FS of the Dirac point to grow and expand around  $K$ , eventually approaching a perfectly nested FS coinciding with the lower vHs for  $t_2 \sim 0.85 t_1$  (Figure 1(c)). This respects the Luttinger theorem, as in a multi-pocket scenario of hole-type and charge-type excitations occupied states can be transferred between the pockets while keeping the total electron number constant. Holes in the lower band around  $K$  are created by shifting the electrons into the upper band at the BZ center. We can interpret  $t_2$  as a pocket-dependent chemical potential shift, since adjusting  $t_2$  has an effective doping effect on the pocket at the BZ boundary.

*Electronic response at vH filling* The combined effect of electronic availability of the vHs and nesting features present on the FS determine viable electronic fluctuation channels, manifest in the static electronic response

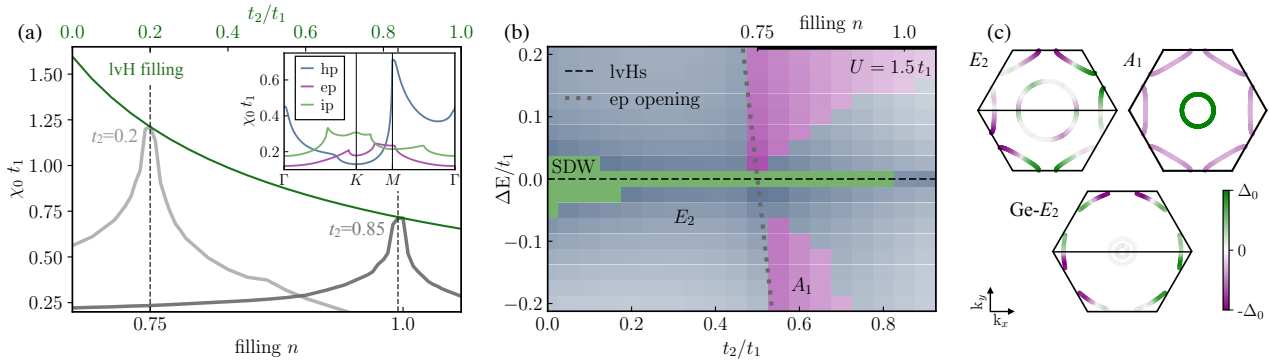


**Figure 2.** *Many body analysis at lower van-Hove singularity.* (a) Leading eigenvalue of the bare susceptibility  $\chi_0$  (Eq. (2)). Both the dependence on  $t_2$  along lower van-Hove (lvH) filling and the doping dependence at fixed long range hopping is depicted. The inset shows the full band-resolved fluctuation spectrum including intra-pocket (ep and hp) and inter-pocket (ip) contributions at  $t_2 = 0.85 t_1$  and  $n = 1.0$ . (b) Resulting phases of Fermi level detuning  $\Delta E$  from lvHs at intermediate interaction scale  $U = 1.5 t_1$ . The intensity of the color indicates the SC pairing strength, which is proportional to the transition temperature  $T_c$ . (c) Superconducting gaps of the chiral  $d$ -wave ( $E_2$ ) and  $s_{\pm}$  ( $A_1$ ) phase, respectively. Each of the two leading basis functions of the inversion odd  $E_2$  irrep is shown in one half of the BZ. Almost identical to the leading  $E_2$  gap function for Germanene structure tuned to vH filling via compressive strain (Ge- $E_2$ , details in SM), the superconducting pairing is exclusively situated on the outer vH pocket. All calculations were performed with  $(800 \times 800)$  integral points and an inverse temperature  $\beta = 250/t_1$  to obtain converged results.

function

$$\chi_{o_1 o_2 o_3 o_4}^0(\mathbf{q}) = -\frac{1}{\beta} \sum_n \int_{\text{BZ}} \frac{d\mathbf{k}}{V_{\text{BZ}}} G_{o_2 o_4}(\mathbf{k}, \omega_n) G_{o_3 o_1}(\mathbf{k} + \mathbf{q}, \omega_n) + \text{h.c.} \quad (2)$$

for the screening of the Coulomb interaction. Here,  $G_{o_1 o_2}(\mathbf{k}, \omega_n)$  is the single particle propagator with momentum  $\mathbf{k}$ , fermionic Matsubara frequency  $\omega_n$  and additional generalized quantum numbers  $o_i$ , incorporating spin and sublattice degrees of freedom. The sum over all frequencies and momenta is normalized by the inverse temperature  $\beta = (k_B T)^{-1}$  and the BZ volume.

The primary contributions to the susceptibility are made by states close to the Fermi level, which means that  $\chi^0$  can be split into three contributions: intra-ep, intra-hp, and ep-hp inter-pocket (ip) scattering channels. We depict this contribution-resolved susceptibility for the example case  $t_2 = 0.85 t_1$  in the inset of Figure 2(a), which is where the vH filling approaches half filling  $n = 1.0$ . The emerging pocket around  $\Gamma$  is a circular ep, where the near isotropy does not promote any distinct transfer momenta  $\mathbf{q}$ . This manifests itself as an absence of distinct peaks in the electronic response [12, 31]. Unlike the Fermiology of pnictides, no nesting exists between the two FS sheets, such that inter-pocket scattering processes are marginal. Hence the dominant fluctuations are exclusively located in the intra-hp scattering channel, where the vHs tuning provides a large DoS to participate in the electronic ordering at the Fermi level, which is concentrated at the  $M$  points of the hexagonal BZ. Accordingly, fluctuations with wavevector  $\mathbf{q} = M$  contain scattering events with

high occupancy of the initial and final states, and thus provide the low-lying fluctuations in the system.

We depict the strength of  $M$  point electronic fluctuations  $\chi^0(M)$  at lower van-Hove (lvH) filling as a measure for the emergence of vHs physics in the honeycomb model (Figure 2(a)). The decreasing DoS at lvH filling, as a function of  $t_2$  (cf. Figure 1(d)), directly translates to the fluctuation strength. However, the fluctuation spectrum appears to be much more susceptible to a violation of the perfect nesting condition: a slight detuning from perfect vHs filling leads to a substantial decrease in the fluctuation strength, as exemplified for two fixed values of  $t_2$  in Figure 2(a). Accordingly perfect nesting plays the primary role in the emergence of electronic order rather than the decay of DoS associated with increasing  $t_2$ .

*Many-body analysis at the compensated metal crossover.* We demonstrate compensated metal ordering tendencies when the single particle states in Eq. 1 are subjected to Hubbard interactions. We model many-body effects within the *random phase approximation* (RPA) [31–35], which focuses on collective particle-hole (ph) excitations as a driver of symmetry breaking transitions. Under this assumption, the full hierarchy of electronic screening processes can be cast into a geometric series that is evaluated analytically. This dresses the ph susceptibility in Eq. 2 to yield the RPA response functions

$$\chi_{c/s}^{\text{RPA}}(\mathbf{q}) = [1 \pm \chi^0(\mathbf{q}) U]^{-1} \chi^0(\mathbf{q}) \quad (3)$$

for charge and spin excitations, respectively. These quantities allow us to probe ph instabilities indicated by a divergent susceptibility channel. At lower scales, however, the RPA provides ph screening for the effective Cooper

pair interaction

$$\Gamma(\mathbf{k}, \mathbf{k}') = U + U\chi^{\text{RPA}}(\mathbf{k} - \mathbf{k}')U - U\chi^{\text{RPA}}(\mathbf{k} + \mathbf{k}')U, \quad (4)$$

which can be evaluated within mean field theory at the Fermi level to reveal the resulting superconducting fluctuations [31]. As a direct consequence of Eq. 3 and the absence of sublattice interference on the honeycomb lattice, the charge response is suppressed by a repulsive interaction  $U > 0$ , and magnetic fluctuations dominate the low energy physics [13]. For  $\chi_s^{\text{RPA}}$ , the higher order screening processes generally increase the imbalance between different momentum channels in the susceptibility. For sufficient interaction scales,  $\chi_s^{\text{RPA}}$  diverges in correspondence to a generalized Stoner criterion, resulting in a spin density wave (SDW) transition.

We presume a generic instability analysis in a small energy window  $\Delta E$  around the lower vHs in the absence of chiral symmetry allowing for charge compensation. Considering previous studies of the honeycomb Hubbard model [12, 13, 15, 36], that consistently find a SDW directly at vH filling, as well as the parameter range suitable for RPA studies, we fix the interaction scale to an intermediate value of  $U = 1.5t_1$  to study the effect of electronic correlations around the Lifshitz transition to compensated metallicity. The minor dependence on the size of the interaction parameter as well as cross-channel effects beyond the RPA are analyzed in detail within the more sophisticated *functional renormalization group* (FRG) scheme in the SM. The FRG allows for an unbiased treatment of superconducting, charge, and magnetic transitions [37–39], that is well suited to treat the competition between SDW and  $d$ -wave SC in graphene at vH filling [12, 13]. We find that the results of RPA and FRG are in good qualitative agreement and only slightly depend on the values of  $U$ . This substantiates the intuitive picture of SC ordering in our model conveyed by our weak coupling analysis employing the RPA formalism.

The landscape of symmetry broken phases around lower vH in Figure 2(b) is dominated by a superconducting phase which transforms according to the  $E_2$  irreducible representation (irrep), displayed in Figure 2(c). The energetically favorable chiral superposition of its two dimensional order parameter gaps out regions of high DoS, *i.e.* areas in the vicinity of the  $M$  points [36]. Our findings agree with previous numerical studies of the  $t_2 = 0$  honeycomb lattice near vH filling and indicate a chiral  $d$ -wave SC [12–14], which remains unaltered in the compensated metal regime. Indicated by its small amplitude the ep barely participates in the pairing process.

While the electronic fluctuation spectrum continues to be dominated by the nesting of the hp, the small Fermi velocity of the ep right above the pocket opening leads to a large DoS at the Fermi level centered around  $\Gamma$ . In this region, the available condensation energy for gapping out the central pocket competes with the electronic fluctuation scales of the hp. A competing  $s_{\pm}$  SC state

(cf. Figure 2(c)) arises close to the pocket opening and is eventually superseded by the  $E_2$  state at sufficient depth of quadratic band dispersion at  $\Gamma$ . Since we are interested in the scenario close to pristine filling around  $t_2 \sim 0.85t_1$  this competitive regime can be safely neglected, and vH-type DoS is identified as the main driver for symmetry breaking in the investigated region of parameter space.

*Strain induced charge compensation in Xene materials*  
The most promising route towards charge compensation in Dirac semi-metals, is buckling: Due to the bipartite unit cell, buckling does not lower the symmetry of the honeycomb layer and provides a generic way to modify monolayer vdW materials through substrate engineering [7, 8]. The decrease of second nearest neighbour distance naturally increases the long range intra sublattice hybridization and highlights the potential of 2D honeycomb layers of the 4th main group like Silicene, Germanene and Stanene, known as *Xenes*, that naturally exhibit buckling due to a  $sp_3$ -like hybridisation process. This buckling tendency can be intensified by utilizing compressive strain originating from a lattice mismatch between Xene-layer and substrate [40–44]. To elevate the proposed charge compensation scheme from analytically traceable tight-binding hamiltonians to real materials, we investigate strained *Xene*-materials by means of density functional theory simulations provided in the supplementary material (SM). The strained Xene structures preserve the dominant FS nesting features of the hexagonal Fermi pocket. Consequently, the observed superconducting order parameters closely resemble the paradigmatic example of the honeycomb Hubbard model at  $t_2 \sim 0.85t_1$  discussed earlier (compare Fig. 2(c)). In addition, the multi-orbital nature of the correlated manifold has a twofold beneficial effect on the charge compensation paradigm: Firstly, additional single particle bands close to the Fermi energy increase the capacity of the spherical charge reservoir at constant energy, such that the required  $t_2/t_1$  ratio at vHs is heavily reduced and eventually reached by small amounts of strain, *e.g.* by a suitable lattice mismatch with the substrate, on which the monolayer is cleaved (cf. SM). Secondly, the orbital separation between  $p_z$  orbitals on the hexagonal pocket and  $sp_2$  derived contributions on the central pockets further suppresses inter-pocket scattering events and further purifies the vH dominated physics in Xene-compounds (cf. SM).

*Conclusion and outlook* For electronic honeycomb lattice models we find strong chiral symmetry breaking due to next-nearest neighbor hopping  $t_2$  as a decisive parameter to tune the filling of the hole-like van-Hove level. The compensating electron-like circular FS pocket in the BZ center due to the Lifshitz transition implied by  $t_2$  does not significantly participate in the symmetry breaking mechanism via many-body effects. Investigating the ordering tendencies of our honeycomb model around half filling with a hole pocket at van-Hove level, we obtain the sought after chiral topological superconducting  $d + id$  instabil-

ity at pristine filling or for moderate doping achievable through methods such as electrolytic gating.

Facing graphene with  $t_2/t_1 \sim 0.15$  [10] as the most appealing electronic honeycomb layer material, this raises the question of how to increase this ratio to the proposed high values  $\gtrsim 0.8$  required to obtain vH physics at pristine filling. Beyond our proposed scheme of facilitating substrate engineered 2D Xene structures, orbital-selective inter-layer hybridization with a substrate or other van-der-Waals (vdW) materials can also promote indirect long range tunneling via external electronic states [45–47]. Another avenue towards strong intra-sublattice hopping on the honeycomb lattice is the realization of large Wannier orbitals like the Fidget spinner states originating from a topological obstruction, that omit the exponential localization of Wannier states at a single lattice site [48].

In this work we discuss chiral symmetry breaking via long ranged hybridization as one mediator inducing compensated metallicity on the honeycomb lattice. However, the presented results rely on the systems fermiology rather than the detailed mechanism of charge compensation. Phenomenologically, this puts compensated metal tuning on the map of correlated quantum material design, which might render itself relevant for future endeavors in stacked multi-layer vdW materials [49, 50].

*Acknowledgement.* We thank J. Heßdörfer, and F. Reinert for discussions. The work is funded by the Deutsche Forschungsgemeinschaft (DFG, German Research Foundation) through Project-ID 258499086 - SFB 1170, and through the research unit QUAST, FOR 5249-449872909 (Project 3 and 5), and through the Würzburg-Dresden Cluster of Excellence on Complexity and Topology in Quantum Matter – *ct.qmat* Project-ID 390858490 - EXC 2147. M.D. received additional funding from the European Research Council under Grant No. 771503 (TopMech-Mat). We acknowledge HPC resources provided by the Erlangen National High Performance Computing Center (NHR@FAU) of the Friedrich-Alexander-Universität Erlangen-Nürnberg (FAU). NHR funding is provided by federal and Bavarian state authorities. NHR@FAU hardware is partially funded by the DFG – 440719683. The authors gratefully acknowledge the Gauss Centre for Supercomputing e.V. (<https://www.gauss-centre.eu>) for funding this project by providing computing time on the GCS Supercomputer SuperMUC-NG at Leibniz Supercomputing Centre (<https://www.lrz.de>).

---

\* Corresponding author: [rthomale@physik.uni-wuerzburg.de](mailto:rthomale@physik.uni-wuerzburg.de)

[1] E. C. Stoner, Collective electron ferromagnetism, *Proceedings of The Royal Society A: Mathematical, Physical and Engineering Sciences* **165**, 372 (1938).

- [2] J. Bardeen, L. N. Cooper, and J. R. Schrieffer, Theory of superconductivity, *Phys. Rev.* **108**, 1175 (1957).
- [3] A. Consiglio, T. Schwemmer, X. Wu, W. Hanke, T. Neupert, R. Thomale, G. Sangiovanni, and D. Di Sante, Van hove tuning of  $av_3sb_5$  kagome metals under pressure and strain, *Phys. Rev. B* **105**, 165146 (2022).
- [4] J. L. McChesney, A. Bostwick, T. Ohta, T. Seyller, K. Horn, J. González, and E. Rotenberg, Extended van hove singularity and superconducting instability in doped graphene, *Phys. Rev. Lett.* **104**, 136803 (2010).
- [5] P. Rosenzweig, H. Karakachian, D. Marchenko, K. Küster, and U. Starke, Overdoping graphene beyond the van hove singularity, *Phys. Rev. Lett.* **125**, 176403 (2020).
- [6] D. Haberer, L. Petaccia, A. V. Fedorov, C. S. Praveen, S. Fabris, S. Piccinin, O. Vilkov, D. V. Vyalikh, A. Preobrajenski, N. I. Verbitskiy, H. Shiozawa, J. Fink, M. Knupfer, B. Büchner, and A. Grüneis, Anisotropic eliashberg function and electron-phonon coupling in doped graphene, *Phys. Rev. B* **88**, 081401 (2013).
- [7] F.-f. Zhu, W.-j. Chen, Y. Xu, C.-l. Gao, D.-d. Guan, C.-h. Liu, D. Qian, S.-C. Zhang, and J.-f. Jia, Epitaxial growth of two-dimensional stanene, *Nature Materials* **14**, 1020 (2015).
- [8] A. Molle, J. Goldberger, M. Houssa, Y. Xu, S.-C. Zhang, and D. Akinwande, Buckled two-dimensional xene sheets, *Nature Materials* **16**, 163 (2017).
- [9] A. H. Castro Neto, F. Guinea, N. M. R. Peres, K. S. Novoselov, and A. K. Geim, The electronic properties of graphene, *Rev. Mod. Phys.* **81**, 109 (2009).
- [10] J. Jung and A. H. MacDonald, Tight-binding model for graphene  $\pi$ -bands from maximally localized wannier functions, *Phys. Rev. B* **87**, 195450 (2013).
- [11] Y. Hatsugai, T. Morimoto, T. Kawarabayashi, Y. Hamamoto, and H. Aoki, Chiral symmetry and its manifestation in optical responses in graphene: interaction and multilayers, *New Journal of Physics* **15**, 035023 (2013).
- [12] R. Nandkishore, L. S. Levitov, and A. V. Chubukov, Chiral superconductivity from repulsive interactions in doped graphene, *Nature Physics* **8**, 158 (2012).
- [13] M. L. Kiesel, C. Platt, W. Hanke, D. A. Abanin, and R. Thomale, Competing many-body instabilities and unconventional superconductivity in graphene, *Phys. Rev. B* **86**, 020507 (2012).
- [14] W. Wu, M. M. Scherer, C. Honerkamp, and K. Le Hur, Correlated Dirac particles and superconductivity on the honeycomb lattice, *Phys. Rev. B* **87**, 094521 (2013).
- [15] W.-S. Wang, Y.-Y. Xiang, Q.-H. Wang, F. Wang, F. Yang, and D.-H. Lee, Functional renormalization group and variational monte carlo studies of the electronic instabilities in graphene near  $\frac{1}{4}$  doping, *Phys. Rev. B* **85**, 035414 (2012).
- [16] A. M. Alsharari and S. E. Ulloa, Inducing chiral superconductivity on honeycomb lattice systems, *Journal of Physics: Condensed Matter* **34**, 205403 (2022).
- [17] F. G. Ribeiro, E. P. Raposo, and M. D. Coutinho-Filho, Competing chiral  $d$ -wave superconductivity and magnetic phases in the strong-coupling hubbard model on the honeycomb lattice, *Phys. Rev. B* **107**, 064510 (2023).
- [18] A. M. Black-Schaffer and S. Doniach, Resonating valence bonds and mean-field  $d$ -wave superconductivity in graphite, *Phys. Rev. B* **75**, 134512 (2007).
- [19] A. M. Black-Schaffer, Edge properties and majorana fermions in the proposed chiral  $d$ -wave superconducting state of doped graphene, *Phys. Rev. Lett.* **109**, 197001

- (2012).
- [20] O. Can, T. Tummuru, R. P. Day, I. Elfimov, A. Damascelli, and M. Franz, High-temperature topological superconductivity in twisted double-layer copper oxides, *Nature Physics* **17**, 519 (2021).
- [21] S. Wolf, T. Gardener, K. L. Hur, and S. Rachel, Topological superconductivity on the honeycomb lattice: Effect of normal state topology, *Phys. Rev. B* **105**, L100505 (2022).
- [22] A. Crépieux, E. Pangburn, L. Haurie, O. A. Awoga, A. M. Black-Schaffer, N. Sedlmayr, C. Pépin, and C. Bena, Superconductivity in monolayer and few-layer graphene. ii. topological edge states and chern numbers, *Phys. Rev. B* **108**, 134515 (2023).
- [23] J. M. Luttinger and J. C. Ward, Ground-state energy of a many-fermion system. ii, *Phys. Rev.* **118**, 1417 (1960).
- [24] J. M. Luttinger, Fermi surface and some simple equilibrium properties of a system of interacting fermions, *Phys. Rev.* **119**, 1153 (1960).
- [25] G. F. Chen, Z. Li, D. Wu, G. Li, W. Z. Hu, J. Dong, P. Zheng, J. L. Luo, and N. L. Wang, Superconductivity at 41 k and its competition with spin-density-wave instability in layered  $\text{ceo}_{1-x}\text{fxFeAs}$ , *Phys. Rev. Lett.* **100**, 247002 (2008).
- [26] X. H. Chen, T. Wu, G. Wu, R. H. Liu, H. Chen, and D. F. Fang, Superconductivity at 43 k in  $\text{smfeaso}_{1-x}\text{fx}$ , *Nature* **453**, 761 (2008).
- [27] M. Rotter, M. Tegel, and D. Johrendt, Superconductivity at 38 k in the iron arsenide  $(\text{ba}_{1-x}\text{k}_x)\text{fe}_2\text{as}_2$ , *Phys. Rev. Lett.* **101**, 107006 (2008).
- [28] A. V. Chubukov, D. V. Efremov, and I. Eremin, Magnetism, superconductivity, and pairing symmetry in iron-based superconductors, *Phys. Rev. B* **78**, 134512 (2008).
- [29] S. Maiti and A. V. Chubukov, Renormalization group flow, competing phases, and the structure of superconducting gap in multiband models of iron-based superconductors, *Phys. Rev. B* **82**, 214515 (2010).
- [30] A. Chubukov, Pairing mechanism in fe-based superconductors, *Annual Review of Condensed Matter Physics* **3**, 57 (2012).
- [31] M. Dürrnagel, J. Beyer, R. Thomale, and T. Schwemmer, Unconventional superconductivity from weak coupling - a unified perspective on formalism and numerical implementation, *The European Physical Journal B* **95**, 112 (2022).
- [32] T. Takimoto, T. Hotta, and K. Ueda, Strong-coupling theory of superconductivity in a degenerate hubbard model, *Phys. Rev. B* **69**, 104504 (2004).
- [33] K. Kubo, Pairing symmetry in a two-orbital hubbard model on a square lattice, *Phys. Rev. B* **75**, 224509 (2007).
- [34] S. Graser, T. A. Maier, P. J. Hirschfeld, and D. J. Scalapino, Near-degeneracy of several pairing channels in multiorbital models for the fe pnictides, *New Journal of Physics* **11**, 025016 (2009).
- [35] M. Altmeyer, D. Guterding, P. J. Hirschfeld, T. A. Maier, R. Valentí, and D. J. Scalapino, Role of vertex corrections in the matrix formulation of the random phase approximation for the multiorbital hubbard model, *Phys. Rev. B* **94**, 214515 (2016).
- [36] A. M. Black-Schaffer and C. Honerkamp, Chiral d-wave superconductivity in doped graphene, *Journal of Physics: Condensed Matter* **26**, 423201 (2014).
- [37] W. H. C. Platt and R. Thomale, Functional renormalization group for multi-orbital fermi surface instabilities, *Advances in Physics* **62**, 453 (2013).
- [38] J. Beyer, J. B. Hauck, and L. Klebl, Reference results for the momentum space functional renormalization group, *The European Physical Journal B* **95**, 65 (2022).
- [39] J. B. Profe, L. C. Rhodes, M. Dürrnagel, R. Bisset, C. A. Marques, S. Chi, T. Schwemmer, R. Thomale, D. M. Kennes, C. A. Hooley, and P. Wahl, Magic angle of  $\text{sr}_2\text{ruo}_4$ : Optimizing correlation-driven superconductivity, *Phys. Rev. Res.* **6**, 043057 (2024).
- [40] A. Acun, L. Zhang, P. Bampoulis, M. Farmanbar, A. Houselt, A. Rudenko, M. Lingenfelder, G. Brocks, B. Poelsema, M. Katsnelson, and H. Zandvliet, Germanene: The germanium analogue of graphene, *Journal of physics. Condensed matter : an Institute of Physics journal* **27**, 443002 (2015).
- [41] L. Zhang, P. Bampoulis, A. N. Rudenko, Q. Yao, A. van Houselt, B. Poelsema, M. I. Katsnelson, and H. J. W. Zandvliet, Structural and electronic properties of germanene on  $\text{mos}_2$ , *Phys. Rev. Lett.* **116**, 256804 (2016).
- [42] J. Li, T. Lei, J. Wang, R. Wu, J. Zhao, L. Zhao, Y. Guo, H. Qian, and K. Ibrahim, Anisotropic electronic structure and interfacial chemical reaction of stanene/ $\text{bi}_2\text{te}_3$ , *The Journal of Physical Chemistry C* **124**, 4917 (2020).
- [43] D. Di Sante, X. Wu, M. Fink, W. Hanke, and R. Thomale, Triplet superconductivity in the dirac semimetal germanene on a substrate, *Phys. Rev. B* **99**, 201106 (2019).
- [44] D. Di Sante, P. Eck, M. Bauernfeind, M. Will, R. Thomale, J. Schäfer, R. Claessen, and G. Sangiovanni, Towards topological quasifreestanding stanene via substrate engineering, *Phys. Rev. B* **99**, 035145 (2019).
- [45] H. Coy Diaz, J. Avila, C. Chen, R. Addou, M. Asensio, and M. Batzill, Direct observation of interlayer hybridization and dirac relativistic carriers in graphene/ $\text{mos}_2$  van der waals heterostructures, *Nano letters* **15** (2015).
- [46] H. C. Diaz, Y. Ma, S. Kolekar, J. Avila, C. Chen, M. C. Asensio, and M. Batzill, Substrate dependent electronic structure variations of van der waals heterostructures of  $\text{mose}_2$  or  $\text{mose}_2(1x)\text{te}_2x$  grown by van der waals epitaxy, *2D Materials* **4**, 025094 (2017).
- [47] Y. Qu, Y. Xu, B. Cao, Y. Wang, J. Wang, L. Shi, and K. Xu, Long-range orbital hybridization in remote epitaxy: The nucleation mechanism of gan on different substrates via single-layer graphene, *ACS Applied Materials & Interfaces* **14** (2022).
- [48] H. C. Po, L. Zou, A. Vishwanath, and T. Senthil, Origin of mott insulating behavior and superconductivity in twisted bilayer graphene, *Phys. Rev. X* **8**, 031089 (2018).
- [49] E. Y. Andrei and A. H. MacDonald, Graphene bilayers with a twist, *Nature Materials* **19**, 1265 (2020).
- [50] T. Devakul, V. Crépel, Y. Zhang, and L. Fu, Magic in twisted transition metal dichalcogenide bilayers, *Nature Communications* **12**, 6730 (2021).
- [51] D. S. de la Peña, J. Lichtenstein, C. Honerkamp, and M. M. Scherer, Antiferromagnetism and competing charge instabilities of electrons in strained graphene from coulomb interactions, *Phys. Rev. B* **96**, 205155 (2017).
- [52] J. C. Meyer, A. K. Geim, M. I. Katsnelson, K. S. Novoselov, T. J. Booth, and S. Roth, The structure of suspended graphene sheets, *Nature* **446**, 60–63 (2007).
- [53] D. Wang, L. Chen, X. Wang, G. Cui, and P. Zhang, The effect of substrate and external strain on electronic structures of stanene film, *Physical chemistry chemical physics : PCCP* **17** (2015).
- [54] J. Gou, L. Kong, H. Li, Q. Zhong, W. Li, P. Cheng, L. Chen, and K. Wu, Strain-induced band engineering

- in monolayer stanene on sb(111), *Phys. Rev. Mater.* **1**, 054004 (2017).
- [55] M. Gmitra, S. Konschuh, C. Ertler, C. Ambrosch-Draxl, and J. Fabian, Band-structure topologies of graphene: Spin-orbit coupling effects from first principles, *Phys. Rev. B* **80**, 235431 (2009).
- [56] M. Bunney, J. Beyer, R. Thomale, C. Honerkamp, and S. Rachel, Chern number landscape of spin-orbit coupled chiral superconductors, arXiv preprint arXiv:2405.03757 (2024).
- [57] S. Wolf, T. Gardener, K. Le Hur, and S. Rachel, Topological superconductivity on the honeycomb lattice: Effect of normal state topology, *Phys. Rev. B* **105**, L100505 (2022).
- [58] G. Kresse and J. Furthmüller, Efficient iterative schemes for ab initio total-energy calculations using a plane-wave basis set, *Phys. Rev. B* **54**, 11169 (1996).
- [59] G. Kresse and D. Joubert, From ultrasoft pseudopotentials to the projector augmented-wave method, *Phys. Rev. B* **59**, 1758 (1999).
- [60] P. E. Blöchl, Projector augmented-wave method, *Phys. Rev. B* **50**, 17953 (1994).
- [61] J. P. Perdew, K. Burke, and M. Ernzerhof, Generalized gradient approximation made simple, *Phys. Rev. Lett.* **77**, 3865 (1996).
- [62] A. A. Mostofi, J. R. Yates, Y.-S. Lee, I. Souza, D. Vanderbilt, and N. Marzari, wannier90: A tool for obtaining maximally-localised wannier functions, *Computer Physics Communications* **178**, 685 (2008).
- [63] The calculation data can be accessed via nomad under <https://dx.doi.org/10.17172/NOMAD/2024.12.19-2>.

# Supplemental Material for Van-Hove tuning of Fermi surface instabilities through compensated metallicity

Hendrik Hohmann,<sup>1,2</sup> Matteo Dürrnagel,<sup>1,2,3</sup> Matthew Bunney,<sup>4,5</sup> Stefan Enzner,<sup>1,2</sup> Tilman Schwemmer,<sup>1</sup> Titus Neupert,<sup>6</sup> Giorgio Sangiovanni,<sup>1,2</sup> Stephan Rachel,<sup>2,4</sup> and Ronny Thomale<sup>1,2,\*</sup>

<sup>1</sup>*Institute for Theoretical Physics and Astrophysics, University of Würzburg, D-97074 Würzburg, Germany*

<sup>2</sup>*Würzburg-Dresden Cluster of Excellence ct.qmat, Germany*

<sup>3</sup>*Institute for Theoretical Physics, ETH Zürich, 8093 Zürich, Switzerland*

<sup>4</sup>*School of Physics, University of Melbourne, Parkville, VIC 3010, Australia*

<sup>5</sup>*Institute for Theoretical Solid State Physics, RWTH Aachen University, 52062 Aachen, Germany*

<sup>6</sup>*Department of Physics, University of Zürich, Winterthurerstrasse 190, Zurich, Switzerland*

(Dated: December 23, 2024)

## Functional renormalization group results

To substantiate our results obtained by large parameter space RPA calculations we employ the functional renormalization group (FRG) for two cross sections of our parameter space, Fig. S1.

The cross sections are taken for two fixed values of  $t_2/t_1 = 0.6, 0.8$ , varying the fillings around the lower van Hove fillings of  $n_{\text{vH}} = 0.845, 0.972$  respectively. The numerics were performed using an established FRG code [38], which was benchmarked against other FRG codes as [51]. This code utilizes the truncated unity approximation of FRG (TUFRG), which assumes that the full two particle interaction vertex is well-approximated by interactions up to a given cutoff range. In this case, the simulations included up fifth-nearest neighbors. The interaction transfer momentum was discretized on a  $36^2$  grid, with a further  $51^2$  refinement used for the calculation of loops and loop derivatives. In order to establish the stability of the phases, calculations were run for several bare values of the on-site Hubbard repulsion  $U$ , from approximately  $1/3 < U/W < 1/2$ , with bandwidth  $W = 8.8 t_1$  for  $t_2 = 0.6 t_1$  and  $W = 10.5 t_1$  for  $t_2 = 0.8 t_1$ .

The results are in qualitative agreement with the RPA data presented in manuscript. In accordance with Figure 2(a), the overall instability scale, measured in the critical cutoff scale  $\Lambda_C$ , decreases as  $t_2/t_1$  increases, which we attribute to a reduced density of states around the Fermi level.

The vHs driven  $E_2$  SC order is more persistent against a detuning from perfect vH filling and the  $A_1$  order is suppressed at intermediate couplings. This is a known drawback of the RPA procedure in the presence of small pockets [39]:

Due to the lack of cross-channel feedback, the RPA overestimates the contributions of ph fluctuations directly at the Fermi level, meaning features of RPA susceptibilities are heavily driven by the fermiology. In the manuscript, RPA sees a superconducting state in the  $A_1$  irrep where the central pocket is small, circular and has a large inverse Fermi velocity. In this case, the  $A_1$  state maximally gaps

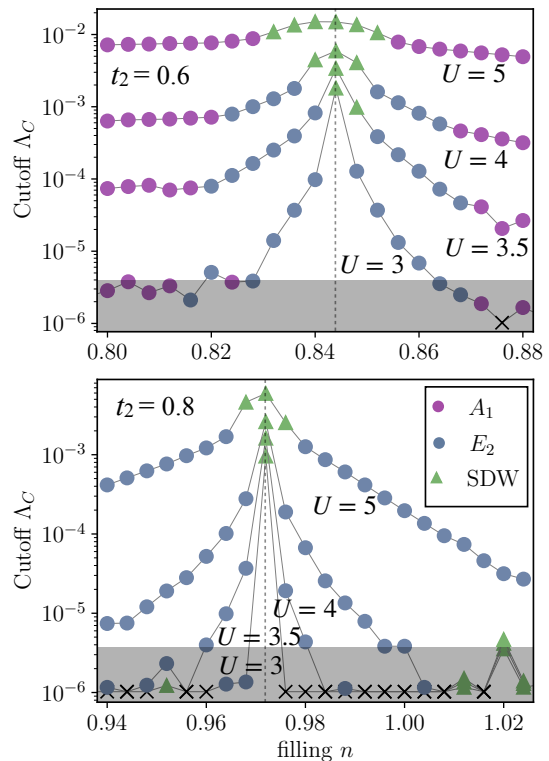


**Figure S1.** Critical cutoffs  $\Lambda_C$  for the leading instabilities in the FRG as a function of onsite repulsion and doping around the lower vHs (dashed line). All values are given in units of  $t_1$ . The gray region indicates where the data becomes unreliable due to finite momentum resolution. The obtained results are consistent with the RPA results presented in Figure 2(b) of the main paper.

out this density of states near the  $\Gamma$  point. What FRG shows is that the van Hove physics can still dominate even if the van Hove singularity is near, but not directly on the Fermi surface, extending the range in filling of the  $E_2$  SC state.

At higher interaction values, the vHs mediated ph fluctuations are directly driving the system into a magnetic Stoner-like instability that is competing with the  $E_2$  SC



order. Hence, at large  $U$  and close to the pocket opening ( $t_2/t_1 \sim 0.55$ ), the  $A_1$  SC phase eventually exceeds the  $E_2$  state and occupies a large part of the phase space away from vH filling.

### Strain induced charge compensation in group-IV 2D-”Xene” materials (X=Si, Ge, Sn)

One promising route to achieve charge compensation in systems with honeycomb structure is buckling. The bipartite unit cell allows for an out-of plane displacement between sublattices without breaking the point group symmetry of the honeycomb layer, as visualized in Fig. S2(a). By shrinking the second nearest neighbour bond length *w.r.t* the nearest neighbour distance, this naturally increases the intra sublattice hybridization and facilitates the charge compensation paradigm due to chiral symmetry breaking.

While the C atoms of graphene stabilize in an almost perfectly flat honeycomb structure (except for potential rippling [52]), its heavier relatives of the main chemical group IV inherently acquire a buckled sublattice structure facilitated by a  $sp_3$ -like hybridization (cf. Fig. S2(b)). This property, however, impedes the synthesis of these materials in a free standing configuration and necessitates a stabilizing substrate to sustain the structure [8]. Experimental and theoretical efforts to realize 2D layers of Silicon, Germanium, and Tin denoted as Xenos (X=Si, Ge, Sn; *i.e.* silicene, germanene, stanene) lead to a variety of possible substrate hosts [7, 41–44]. As most of the works focus on maintaining and utilizing the topological features concentrated around 2D Dirac cones, our charge compensation paradigm reveals a novel avenue for experimental investigations of Xene compounds: As demonstrated in many systems, the lattice mismatch can be utilized to induce compressive (or tensile) strain within the Xene structure, eliciting an increased (decreased) buckling [8, 43, 53, 54]. Consequently, the intra-sublattice hybridization increases and facilitates effective charge compensation under compressive strain. Previously, the resulting displacement of the Fermi level was considered as a disadvantage as it inhibits the QSH insulator phase in favor of a metallic state. However, the metallic phase enables a topological SC transition, as proposed in this manuscript.

We conducted comprehensive DFT studies of silicene, germanene, and stanene under compressive strain. As displayed in Fig. S2(c), van-Hove filling at charge neutrality is obtained for 5% to 9% compression of the free standing lattice constant, which is in a order of magnitude proven to be experimentally accessible via epitaxial growth on *e.g.* a  $\text{MoS}_2$  or  $\text{Bi}_2\text{Te}_3$  substrate [7, 8, 41, 43]. Deviating from the Honeycomb model employed in the main text, the Xene eigenspectra in Fig. S2(d) feature an additional band stemming from  $sp_2$ -derived hybrid

orbitals, that eventually crosses the Fermi level close to  $\Gamma$ . This leaves the vH singularity at pristine filling unaltered while providing an additional hole pocket contributing in the charge compensation. Thereby, the required long range hybridisation and hence strain for perfect charge compensation at van-Hove is considerably reduced compared to the honeycomb Hubbard model discussed in the main text.

### Orbital selectivity and robust $E_2$ superconductivity in Xene compounds

Analogous to the fermiology of the honeycomb Hubbard model at  $t_2/t_1 \sim 0.85$ , the strained Xene structures preserve the dominant FS nesting features of the outer hexagonal Fermi pocket accountable for the vHs. Despite the pronounced hexagonal shape of the additional hole-pocket, its integrated density of states is small and we expect the vH pocket to be the main driver for symmetry breaking transitions in the Xene compounds. This suspicion is enhanced by an inspection of the orbital character of the FS states in germanene: As evident from Fig. S3, the  $p_z$  orbital is predominantly contributing to the outer Fermi pocket. Hence, the imbalance between intra and inter-pocket scattering from poor FS nesting is further enhanced by not matching orbital makeup of the low lying electronic states. This property is recovered qualitatively for the three Xene materials under investigation.

We take into account the multi-orbital nature of the Xene valence bands by defining orbital dependent intra-orbital interactions. Since the  $sp_2$  orbitals are binding orbitals, that constitute the chemical bonds of the crystal lattice, we expect larger screening of the Coulomb repulsion and less impact on symmetry breaking transitions for these orbitals. Hence, we set  $U_{p_z} = 1.5\text{eV}$  for the  $p_z$  orbital and neglect the interaction within the  $sp_2$  manifold.

Determining the superconducting phase for strained Xene structures at van-Hove filling within the random phase approximation reveals robust  $d$ -wave gaps transforming within the  $E_2$  irrep. The order parameter in Fig. 2 of the main paper resembles the main features of the charge compensated honeycomb model: The gap function allows for a topological  $d + id$  SC state, that gaps out the outer Fermi pocket completely, while the two hole-pockets are barely participating in the pairing process.

### Effect of spin orbit coupling

As evident from our ab-initio analysis (cf. Fig. S2(d)), Xene structures consisting of heavier atoms require less strain to reach the charge compensated regime. This comes at the expense of having sizable spin-orbit coupling

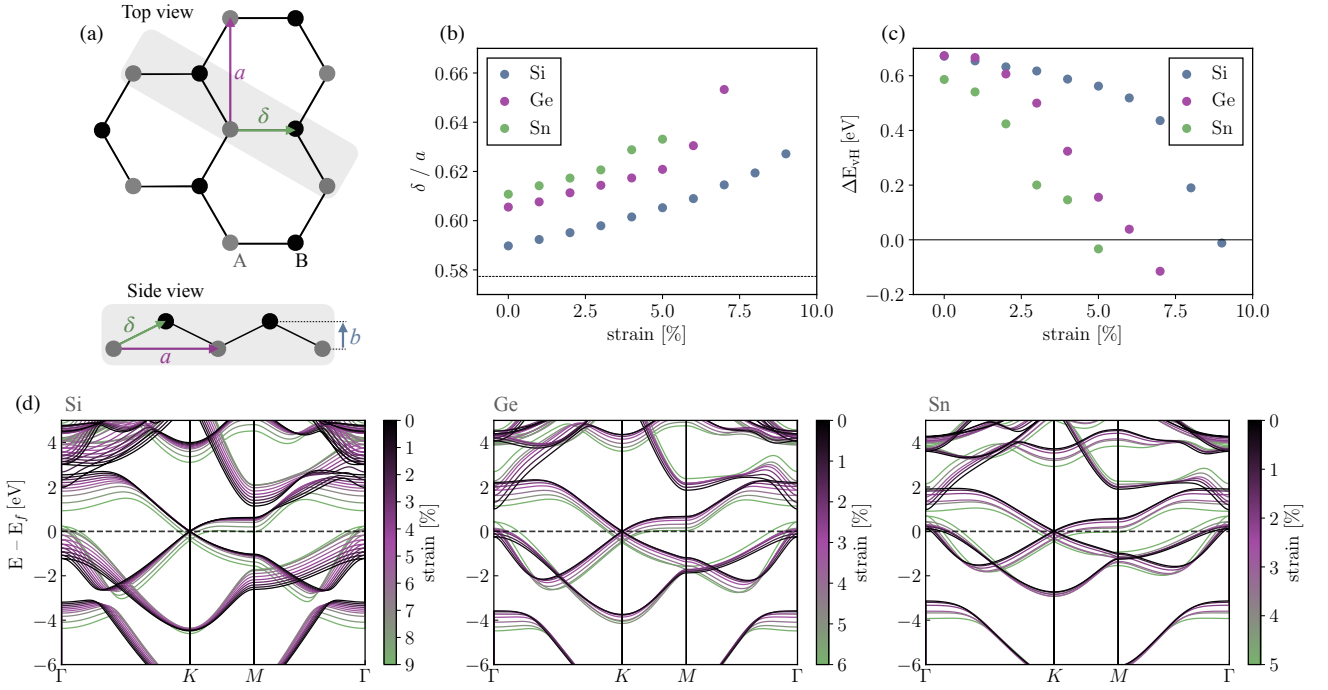


**Figure S2.** Xene lattice parameter with applied biaxial strain. (a) Real space position of the honeycomb sublattice sites in a buckled structure with (next) nearest neighbour distance  $\delta$  ( $a$ ). (b) Dependence of relative bond lengths for the Xene structures silicene, germanene and stanene on strain. The strain is quantified as the enforced relative compression of the lattice constant of the fully relaxed structure. The black line indicates the  $\delta/a$  ratio for the ideal honeycomb structure considered in the main text. (c) Energy offset of the upper van-Hove point from the Fermi level as a function of compressive strain for the different Xene compounds. (d) Density functional theory band structures of silicene (Si), germanene (Ge), and stanene (St) for different values of strain. The dashed line indicates pristine half filling for each strain value individually.

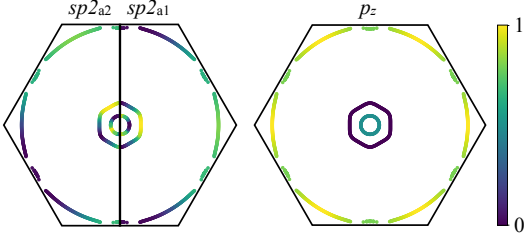


**Figure S3.** Orbital character on the FS for germanene strained by 6%. Two exemplary  $sp_2$  orbitals are shown on the left. The  $p_z$  orbital is mainly contributing to the outer Fermi pocket that is facilitating the  $E_2$  SC phase. These properties are recovered qualitatively by silicene and stanene.

(SOC), therefore deviating from the paradigmatic example of Xenos, i.e. graphene. Our relativistic density functional theory calculations indicate a gap opening at the Dirac points with increasing gap size for increasing SOC. Our DFT calculations for unstrained silicene, germanene, and stanene reveal a gap at the Dirac points of  $\approx 0.002$  eV,  $\approx 0.024$  eV, and  $\approx 0.077$  eV, respectively. Conversely, the vHs at the  $M$ -points remain spin degenerate. For strained Xenos, however, Rashba-type SOC emerges due to the

buckled structure [55] which breaks inversion symmetry and would, in principle, allow for mixing of singlet and triplet superconducting states. It was recently shown that on hexagonal lattices such singlet-triplet mixing indeed occurs in the presence of Rashba SOC, but the  $E_2$  irrep and chiral superconductivity prevail [56]. Moreover, the emergent Rashba SOC induces a spin splitting at the vHs [55] which, according to our DFT calculations, is negligible in the present case. As long as this gap is small, it was shown that the superconducting states nearby are not affected [57].

### Details of density functional theory calculations

The DFT calculations were performed with the Vienna ab initio simulation package (VASP) [58] within the projector augmented-plane wave (PAW) method [59, 60]. For the exchange-correlation potential the PBE-GGA functional [61] was used, by expanding the Kohn-Sham wave functions into plane waves up to an energy cutoff of 400 eV. We sample the Brillouin zone on a  $12 \times 12 \times 1$  Monkhorst-Pack mesh. We considered the free-standing buckled monolayers silicene, germanene and stanene. To avoid unwanted interactions between adjacent sheets a

vacuum distance of 15Å was employed. The structures are relaxed in the out-of-plane direction until forces converged below 0.01 eV/Å. With Wannier90 8-orbital tight binding

Hamiltonians were derived for the  $p_z$  and the  $sp_2$  hybrid orbitals [62]. The input files of the density functional theory calculations are publicly available [63].